Supplemental Figure 1

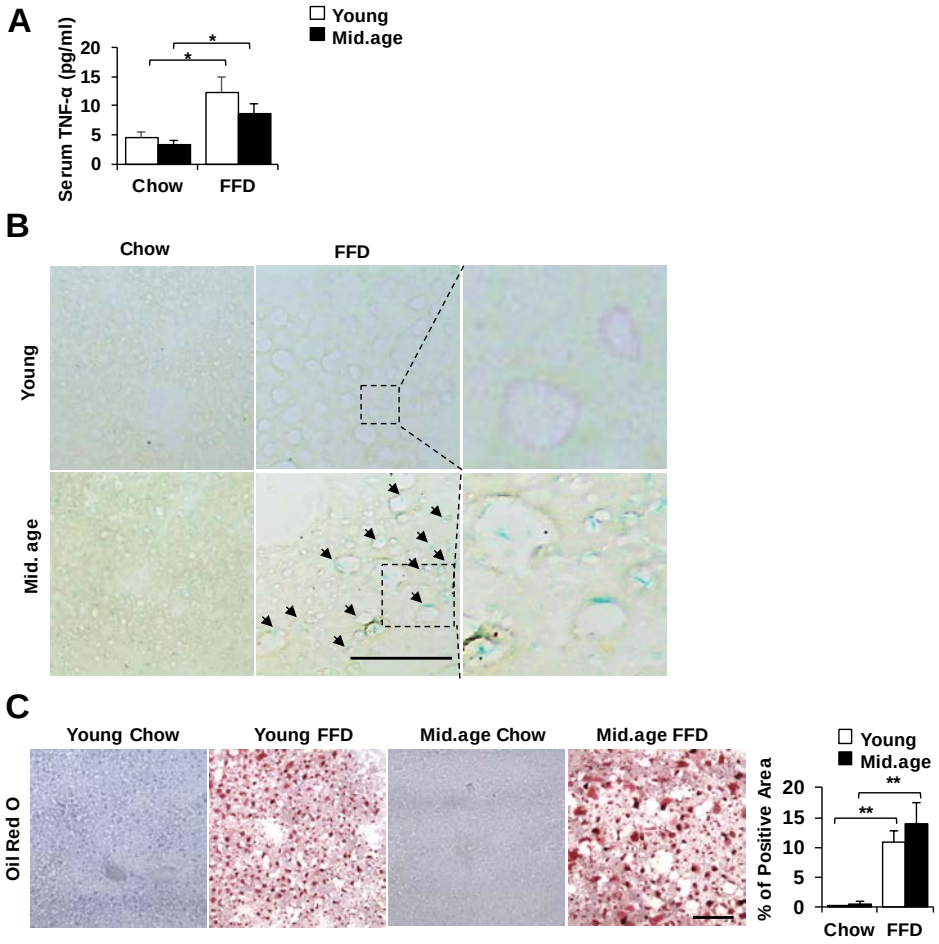

Suppl. Fig. 1. Middle-aged mice on fast food diet have an increase in senescence and steatosis.

Young (6-week, at the beginning of FFD), and middle-aged mice (26-weeks) were fed the FFD for 18 weeks, and serum TNFα tested by ELISA showed an increase in both young and middle aged mice on FFD albeit the difference between ages was not significant (**A**). To further evaluate senescence, SA-β galactosidase (**B**) was tested. Middle-aged mice on FFD had positive signal for SA-β galactosidase (arrows) while this was rare in young mice on FFD. On oil-red staining, steatosis has increased in middle-aged mice as assessed by NIH ImageJ analysis. (The percentage of positive staining area per 20x field was quantified with ImageJ from 4 random fields of 3-6 mice in each group, respectively **C**). Mean±SEM, N=5-7, *p<0.05, **p<0.01.

Supplemental Figure 2

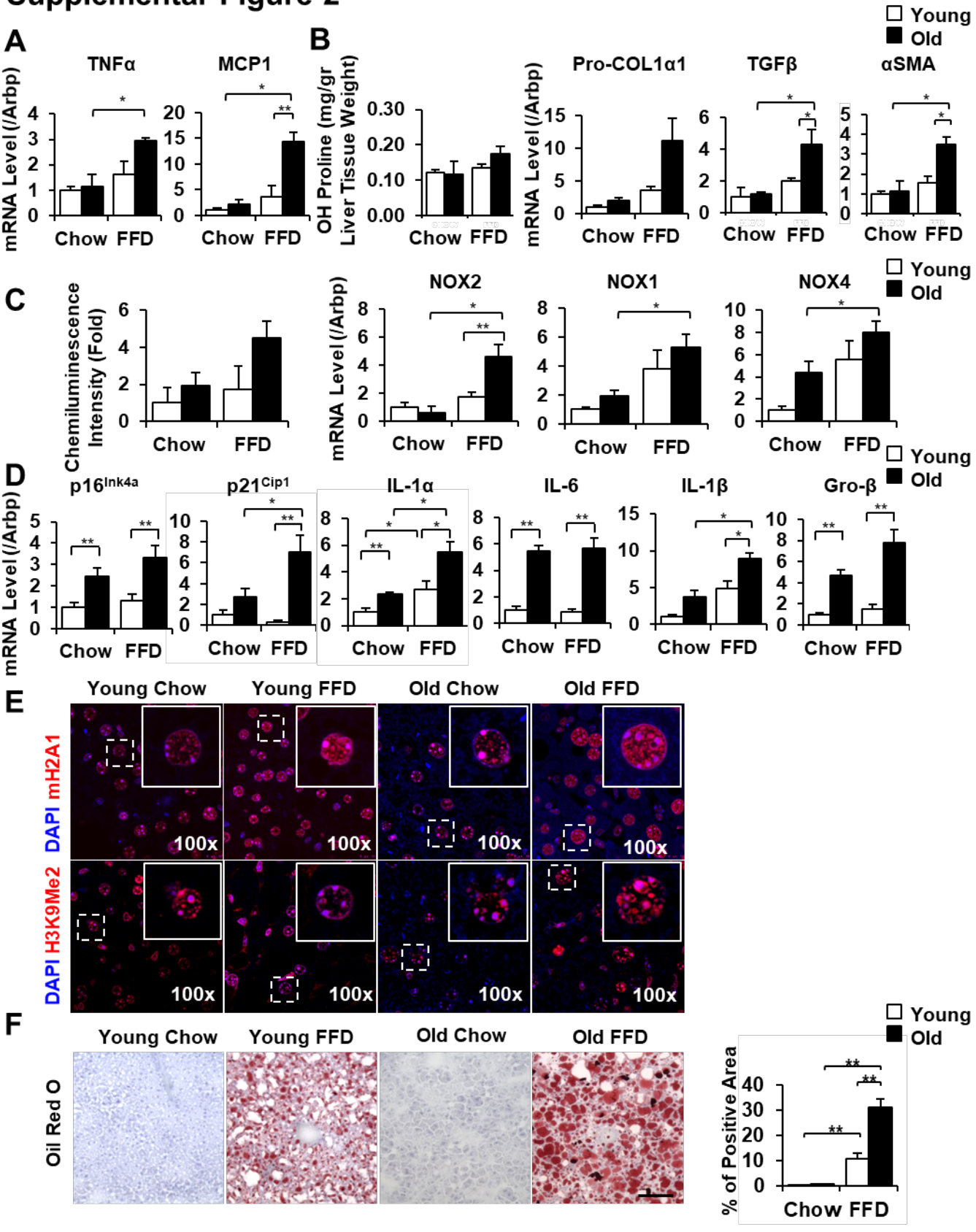

Suppl. Fig. 2. Old mice have more necroinflammation, fibrosis and significant increase in senescent cells on fast food diet. Young (6-week, at the beginning of FFD), and old mice (48-weeks) were fed FFD for 8 weeks (we chose shorter feeding, as older mice may not survive longer NASH feeding). Old mice exhibited significant increase in mRNA for TNFα, and MCP-1 **(A)**. Hydroxy-proline content, mRNAs for procollagen I, TGF-β, and α-SMA increased in old, compared to young mice on FFD (**B**). ROS, and NOX2 were more significantly induced on FFD in old mice whereas the non-phagocytic NOX1 and 4 isoforms showed no significant induction over that observed in young mice (**C**). Senescence markers $p16^{INKa}$ and $p21^{Cip1}$ were significantly induced and there was a significant activation of SASP (IL-1α, IL-6, IL-1β and Gro-β (**D**). SAHF marks (mH2A1 and H3K9Me2/3) showed an increase in old mice (**E**). Oil red staining demonstrated increased steatosis in old mice even after a short course of FFD, assessed by ImageJ (The positive staining area was quantified in 4 random fields of 3-6 mice in each group, respectively. **F**) (Mean±SEM, N=5-7, *$p<0.05$, **$p<0.01$).

Supplemental Figure 3

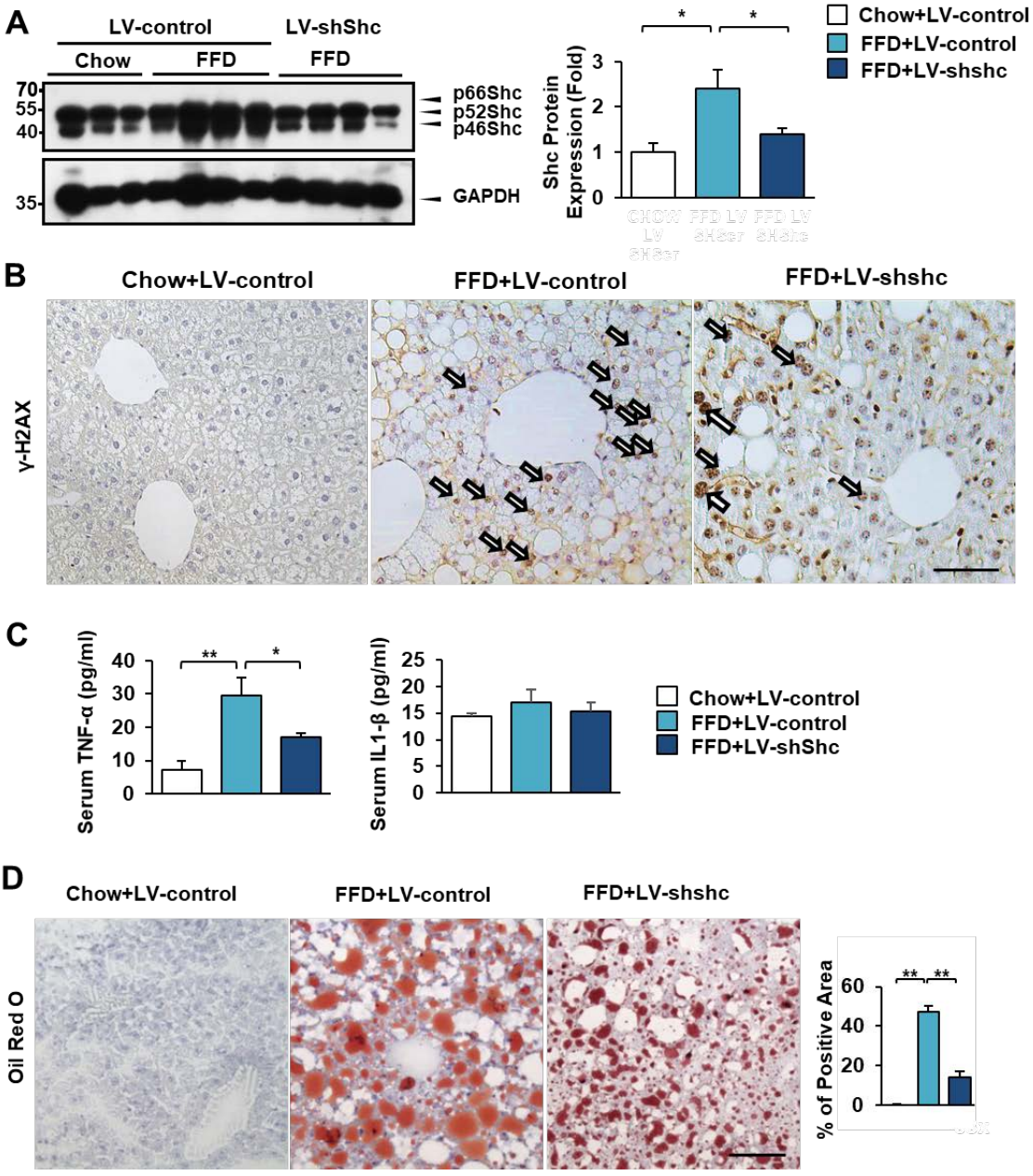

Suppl. Fig. 3. LV-shShc-injected mice display improved γH2AX and steatosis.

48w old mice were placed on FFD and injected by LV-ShScr or LV-ShShc at week 9 of the 18w diet. P46 and p42Shc were induced by FFD, and in mice transduced by LV-shRNA there was a reduction of Shc, as assessed by densitometry (**A**).

To further study senescence, we assessed γH2AX (senescence marker, DNA strand break) and found more nuclei with γH2AX marks (arrows) in scrambled ShRNA transduced livers than in

ShShc transduced ones (**B**). ELISA for TNFα shows significant reduction in ShRNA-transduced mice however serum IL-1β was not different (**C**). Oil red staining depicts increased steatosis in LV-ShScr transduced old mice after FFD that improved after LV-SH-Shc injection, as assessed by ImageJ (quantified in 4 random fields of 3-6 mice in each group, respectively, **D**).

(Mean±SEM, N=5-7, *$p<0.05$, **$p<0.01$).

Supplemental Figure 4

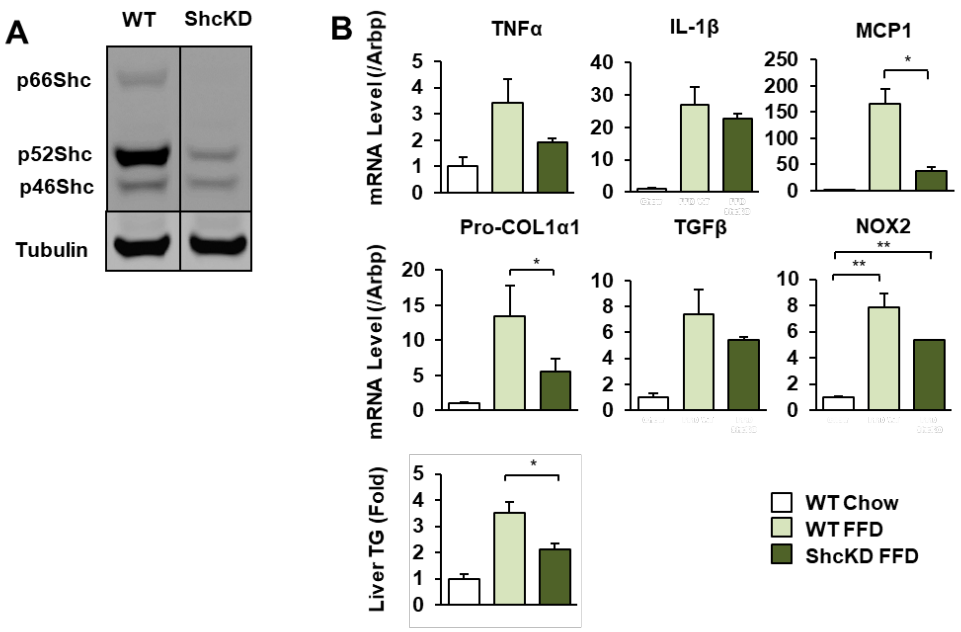

Suppl. Fig 4. ShcKD mice are protected from diet-induced NASH. Western blot from wt and ShcKD livers demonstrate that ShcKD mice have not only reduced p66Shc, they also have much decreased levels of p52Shc and p46Shc in the liver (**A**). We placed littermate ShcKD vs. control mice on FFD for 18w. TNFα, IL-1β MCP-1, and fibrogenic transcripts procollagen-α1(I), TGFβ were reduced, and TG content and NOX2 were lower in ShcKD mice (**B**, Mean±SEM, N=3-4, *p<0.05).

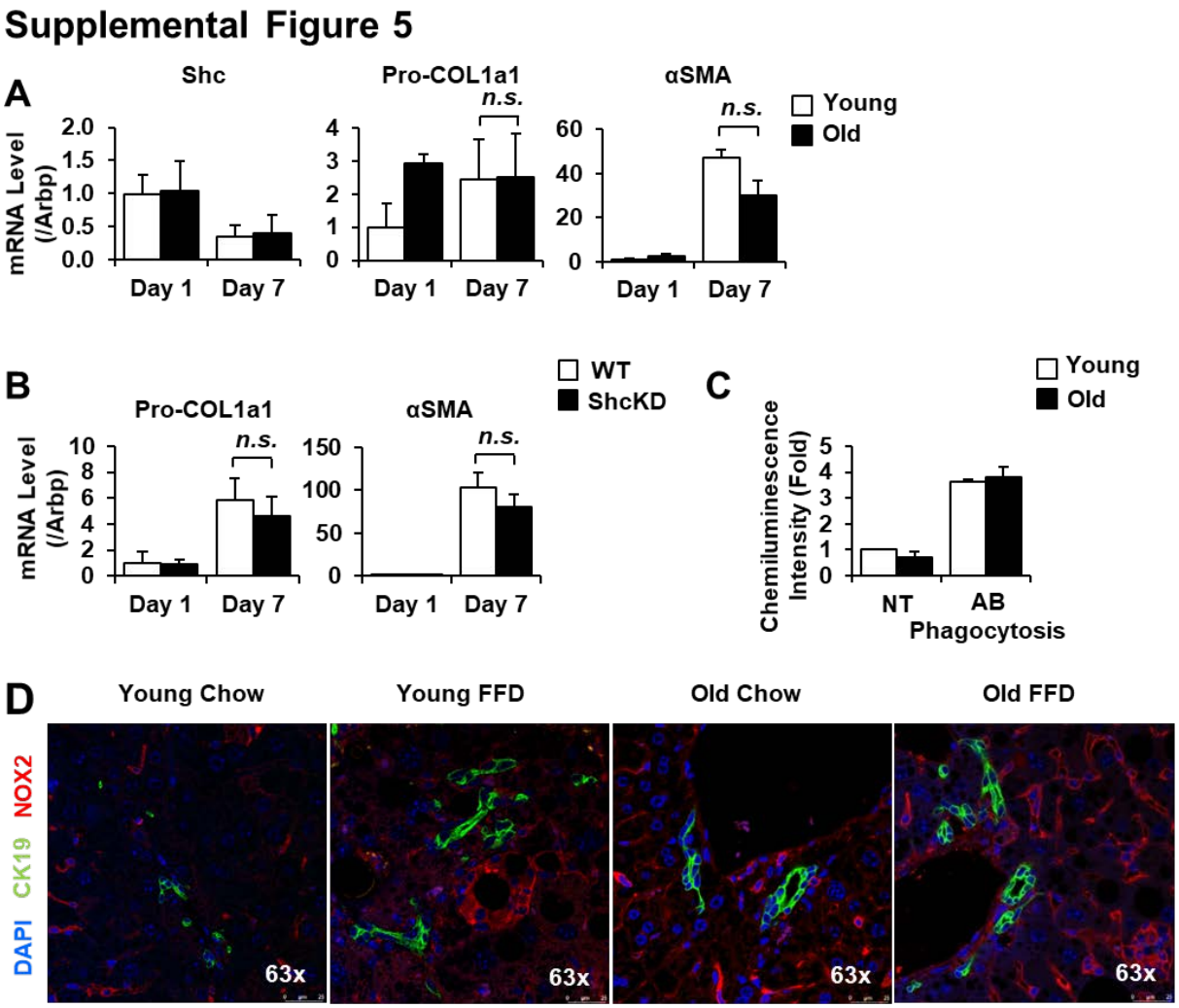

Suppl. Fig. 5 Shc is not required for HSC culture-activation or NOX2-mediated oxidative burst upon efferocytosis in macrophages.

Primary HSC were isolated from young (6w) and old (20m) wt mice. Shc expression and culture activation showed no difference between young/old cells (**A**), and Shc was not required for culture activation of HSC (**B**). Respiratory burst following phagocytosis of apoptotic bodies was not different in young vs. old liver macrophages (**C**). Macrophages isolated from young and old mice were exposed to hepatocyte apoptotic bodies (AB), and ROS production was measured by the lucigenin assay. We did not detect significant difference between the age groups (Mean±SEM, N=3, *n.s.*: non-significant). CK19 (green) and NOX2 (red) immunostaining did not reveal colocalization by confocal microscopy (**D**)

Supplemental Figure 6

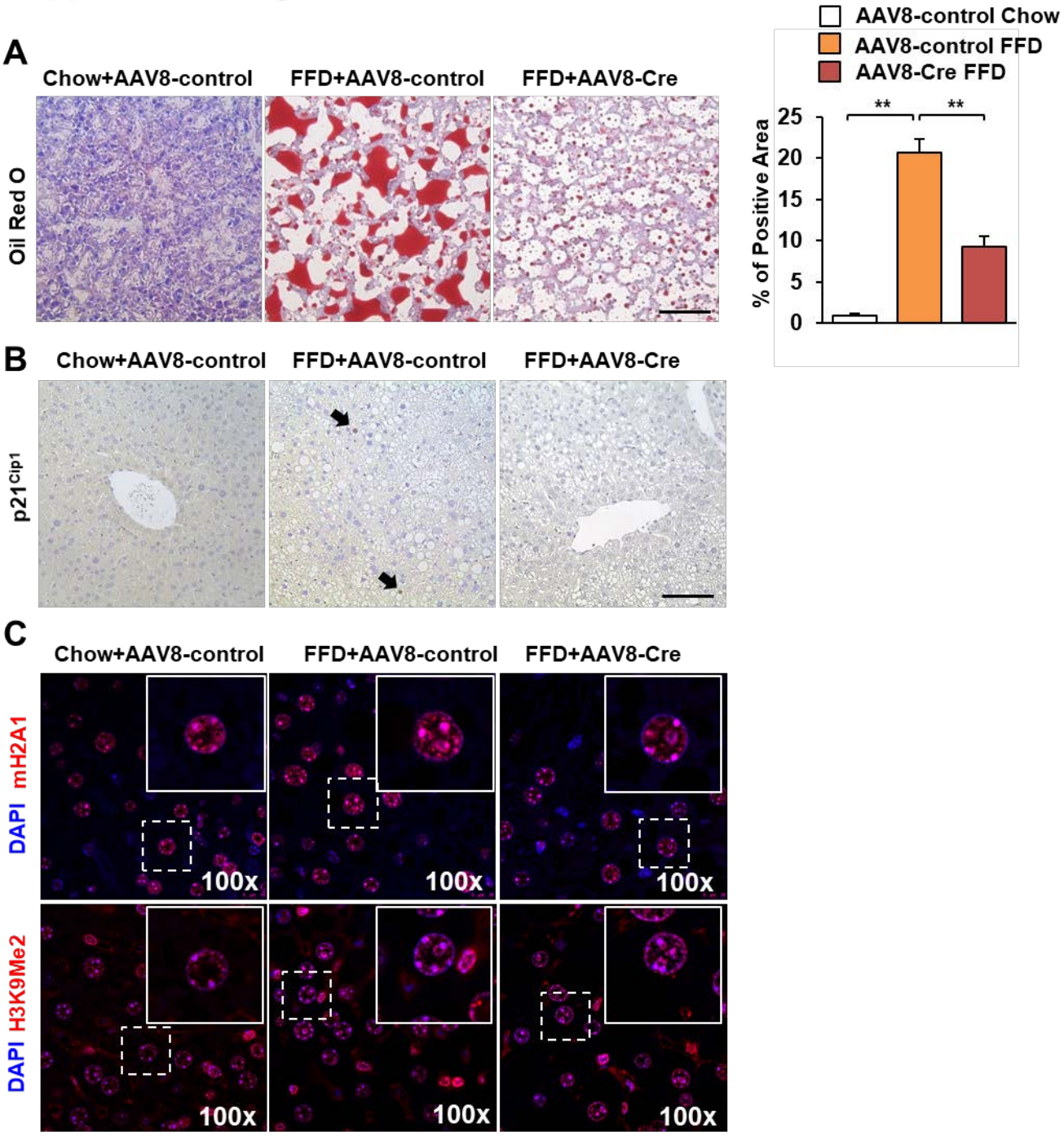

Suppl. Fig 6. Hepatocyte Shc-deleted mice display decreased steatosis but no significant changes in senescence markers.

12w-old *fl/fl* Shc mice were placed on either chow or FFD. At week 9 of the 18w FFD a group of *fl/fl* mice were injected with either AAV8-GFP (control) or AAV8-TBG-Cre, *via* the tail vein. Oil-red stain shows an increase in steatosis in AAV8-GFP-injected mice that has improved after

hepatocyte Shc deletion, as assessed by Image J analysis. (Quantification from 4 random fields of 3-6 mice in each group, respectively. (**A)** Mean ± SEM, N=5-7, **p<0.01). Marker of senescence $p21^{Cip1}$ nuclear staining did not show an increase in FFD fed young mice (**B**), but SAHF depict early changes with increasing histone marks (**C**).

Supplemental Figure 7

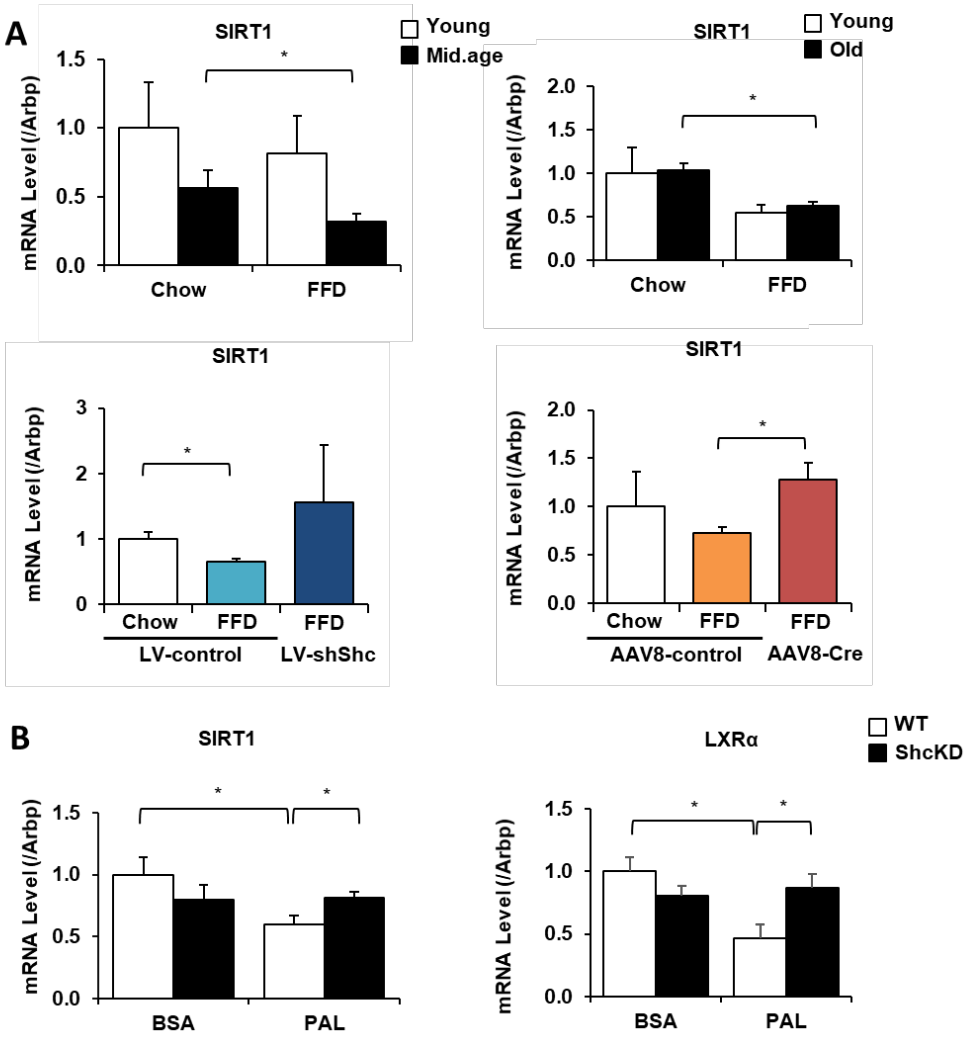

Suppl. Fig. 7 Sirtuin 1 is downregulated in older mice in a Shc-dependent manner.

We tested Sirt1 expression in middle-aged mice on FFD, in old mice injected with LV-Scr or LV-Shc, and in conditional hepatocyte KO mice. Sirt1 was downregulated at an older age in NASH, and Shc inhibition or deletion from hepatocytes showed reversal of these findings (**A,** Mean±SEM, N=3-7, *p<0.01). In primary hepatocytes isolated from middle-aged wt or ShcKD mice and treated with palmitate, Shc was downregulated and this was reversed in KD cells. LXRα expression was also improved in ShcKD cells, exposed to palmitate (**B**, Mean±SEM, N=3, *p<0.05).

Supplemental Figure 8

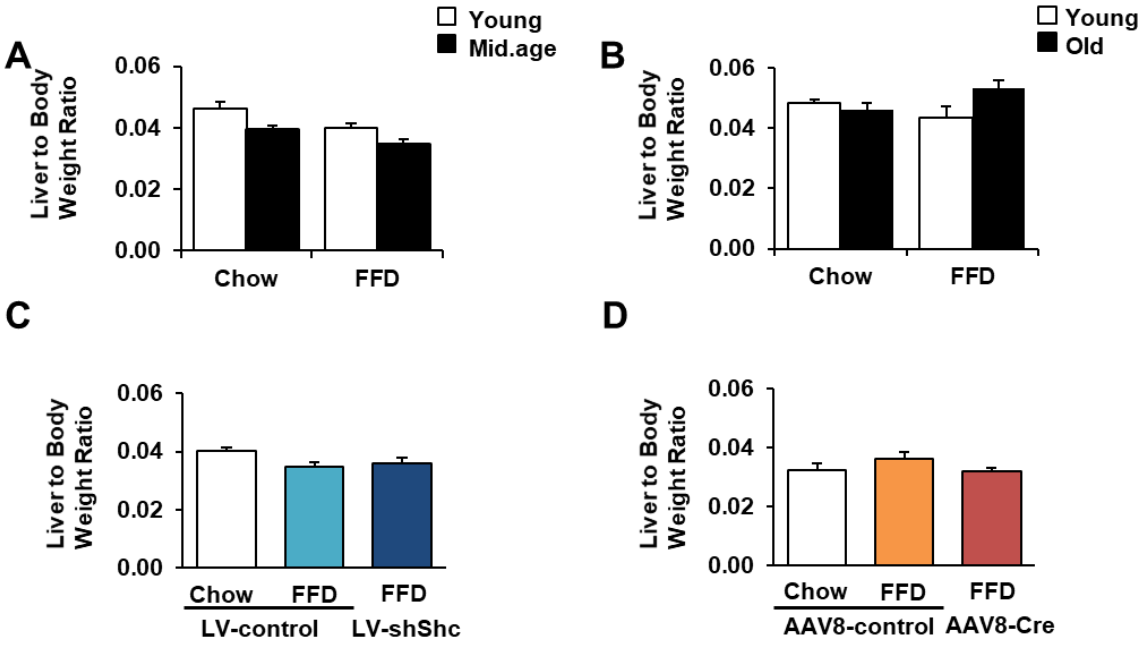

Suppl. Fig. 8 Liver to Body Ratios in each model

We calculated the ratio of the liver weight over body weights of the mice in all our feeding cohorts, and plotted the average ratios. We did not observe any significant change in liver/body weight ratios (Mean±SEM, N=3-7).

Supplementary Table 1. Patient Sample Data

Normal		NASH Patients			
Age	**Gender**	**Age**	**Gender**	**NAS Score**	**Fibrosis**
23	F	12	M	5	3
32	F	32	F	7	4
43	F	36	M	5	0
44	M	39	M	4	1
50	M	47	M	7	0
65	M	55	F	5	0
69	F	62	F	6	2
71	M	63	F	4	0
77	M	83	F	5	1
85	F				

For normal samples we used resection samples from peritumoral tissues (with normal histology). NASH samples were either resection samples (frozen, processed for WB), or biopsy samples.

NAS score: 4-7, and fibrosis stage 0-4.

Supplementary Table 2. Summary of Primers for RT-PCR

Gene	Sequence
Mouse Arbp	Forward: 5’-CAAAGCTGAAGCAAAGGAAGAG-3’ Reverse: 5’-AATTAAGCAGGCTGACTTGGTTG-3’
Mouse α-SMA	Forward: 5’-GTTCAGTGGTGCCTCTGTCA-3’ Reverse: 5’- ACTGGGACGACATGGAAAA-3’
Mouse Pro-Col1α1	Forward: 5’-AGAGGCGAAGGCAACAGTCG-3’ Reverse: 5’- GCAGGGCCAATGTCTAGTCC-3’
Mouse Gro-β	Forward: 5’-GTGAACTGGGCTGTCAATG-3’ Reverse: 5’-GGCGTCACACACTCAAGCTCT-3’
Mouse IL-1α	Forward: 5’-GGGTGACAGTATCAGCAACG-3’ Reverse: 5’-GACAAACTTCTGCCTGACGA-3’
Mouse IL-1β	Forward: 5’-CAACCAACAAGTGATATTCTCCATG-3’ Reverse: 5’-GATCCACACTCTCCAGCTGCA-3’
Mouse IL6	Forward: 5’-TTCCATCCAGTTGCCTTCTTG-3’ Reverse: 5’- GAAGGCCGTGGTTGTCACC-3’
Mouse LXRα	Forward: 5’-TCAATGCCTGATGTTTCTCCTG-3’ Reverse: 5’-CTCCAACCCTATCCCTAAAGC-3’
Mouse MCP1	Forward: 5’-CTTCTGGGCCTGCTGTTCA-3’ Reverse: 5’-CCAGCCTACTCATTGGGATCA-3’
Mouse NOX1	Forward: 5’-CAGAAGCGAGAGATCCATCCA-3’ Reverse: 5’-CAGTTATTCATATCATTGCACACCTATTT-3’
Mouse NOX2	Forward: 5’-CCCTTTGGTACAGCCAGTGAAGAT-3’ Reverse: 5’-CAATCCCGGCTCCCACTAACATCA-3’
Mouse NOX4	Forward: 5’-TTGCCTGGAAGAACCCAAGT-3’ Reverse: 5’-TCCGCACAATAAAGGCACAA-3’
Mouse $p16^{lnk4a}$	Forward: 5’-CGTACCCCGATTCAGGTGAT-3’ Reverse: 5’-TTGAGCAGAAGAGCTGCTACG T-3’
Mouse $p21^{Cip1}$	Forward: 5’-GAGGCCCAGTACTTCCTCT-3’ Reverse: 5’-CTGCGCTTGGAGTGATAGA-3’
Mouse Shc	Forward: 5’-CGTCTCCCGTATTCTCTAACTT-3’ Reverse: 5’-GCCACTCCTGTCCCTATTCTCC-3’
Mouse Sirt1	Forward: 5’-CTCTGAAAGTGAGACCAGTA-3’ Reverse: 5’-TGTAGATGAGGCAAAGGTTC-3’
Mouse TGF-β	Forward: 5’-TGGAGCAACATGTGGAACTC-3’ Reverse: 5’-CAGCAGCCGGTTACCAAG-3’
Mouse TNF-α	Forward: 5’-TCCCAGGTTCTCTTCAAGGGA-3’ Reverse: 5’-GGTGAGGAGCACGTAGTCGG-3’
Human 18s	Forward: 5’-GGCCCTGTAATTGGAATGAGTC-3’ Reverse: 5’-CCAAGATCCAACTACGAGCTT-3’
Human Shc	Forward: 5’-CCAGTATGTGCTCACTGCT-3’ Reverse: 5’-CTTAGTCCGAACCACACCCT-3’

Supplementary Table 3. Summary of Antibodies

Name	**Manufacturer/ Cat #**	**Application/ Concentration**
Primary Antibodies		
Shc	BD, #610878	WB, 1:1000
p47phox (phospho-Ser 370)	Syd Labs, #PA002881-A1171	WB, 1:1000
Gp91-phox (54.1)	Santa Cruz, #sc-130543	WB, 1:200 - IP, 1:50 IF, 1:50
p-Ser (16B4)	Santa Cruz, #sc-81514	WB, 1:200
Albumin	Bethyl Laboratories, # A90-134A	IF, 1:200
F4/80 (clone Cl:A3-1)	BIO-RAD, # MCA497RT	IF, 1:100 IHC, 1:100
CK19 (BA-17)	Abcam, #ab7755	IF, 1:100
CK19 (EPNCIR127B)	Abcam, #ab133496	IHC, 1:1000 IF, 1:500
Shc [EP332Y]	Abcam, #ab33770	IHC, 1:100 IF, 1:100
4-Hydroxynonenal (4-HNE)	Abcam, #ab46545	IHC, 1:500
gamma H2AX	Abcam, #ab26350	IHC, 1:250
macro H2A1	Abcam, #ab37264	IF, 1:250
H3K9Me2	Abcam, #ab1220	IF, 1:250

Supplementary Table 3 (cont.). Summary of Antibodies

Name	**Manufacturer/ Cat #**	**Application/ Concentration**
Secondary Antibodies		
HRP Goat α-Mouse	EMD Millipore, #710453	WB, 1:5000
HRP Goat α-Rabbit	Abcam, #ab6721	WB, 1:5000
Alexa Fluor 555 Goat α-Mouse	Invitrogen, A21422	IF, 1:500
Alexa Fluor 555 Donkey α-Rabbit	Invitrogen, A31572	IF, 1:500
Alexa Fluor 488 Donkey α-Mouse	Invitrogen, A21202	IF, 1:500
Alexa Fluor 488 Chicken α-Rabbit	Invitrogen, A21441	IF, 1:500
Alexa Fluor 488 Chicken α-Goat	Invitrogen, A21467	IF, 1:500
Alexa Fluor 488 Goat α-Rat	Invitrogen, A11006	IF, 1:500
Biotinylated Goat α-Mouse	Vector Lab,#BA-9200	IHC, 1:500
Biotinylated Goat α-Rabbit	Vector Lab,#BA-1000	IHC, 1:500
Biotinylated Goat α-Rat	Vector Lab,#BA-9400	IHC, 1:500

Supplementary Table 4. Solvent Accessible Surface Area (SAS) Interface of p52Shc to the p47^{phox}

Solvent accessible surface area	p47^{phox} (Å^2)	p52Shc (Å^2)	Complex (Å^2)	Interface (Å^2)
Dock1	30990	34521	64466	1045
Dock2	30990	34577	64917	650

Cell isolation and culture. Primary hepatocytes were isolated following collagenase reverse perfusion as previously described (1). Cells were cultured in William's E Medium (Sigma-Aldrich) with 10% FBS and antibiotics. Primary stellate cells were isolated from mice as described previously (2), and cultured in Medium 199 (Sigma-Aldrich, St. Louis, MO) with 20% fetal bovine serum (FBS, Gibco®- Thermo Fisher Scientific, Waltham, MA) and antibiotics. Liver macrophages were isolated as previously described (3), and were cultured in RPMI (Gibco®) with 10% FBS and antibiotics. HEK293 and HepG2 cells (American Type Culture Collection, Manassas, VA) were maintained in DMEM supplemented with 10% FBS and antibiotics.

Histology, immunohistochemistry, immunofluorescence, and oil red O staining. NAS scores (inflammation, hepatocyte ballooning and steatosis) and fibrosis stages were evaluated for each experimental model by a liver pathologist in a blinded fashion. Paraffin-embedded slides were deparaffinized and rehydrated. For antigen retrieval, they were boiled in citrate buffer (0.01 M, pH 6.0). After incubation in 3% aqueous H_2O_2 to quench endogenous peroxidase, sections were washed in 0.1% Triton X-100 in PBS, and blocked with 5% goat serum (EMD Millipore, Burlington, MA) in wash buffer. Sections were then sequentially incubated with primary and secondary antibodies (Supplementary Table 3). For immunohistochemistry, the slides were treated with diaminobenzidine substrates (Abcam) to visualize the signal and counterstained with Mayer's hematoxylin (Fisher). Images were taken with Leica DM2000 (Leica Microsystems Inc., Buffalo Grove, IL) or scanned with Leica Aperio AT2 at Stanford Human Pathology /histology service center. NIH Image J software was used to count the signal and the average counts were used to plot the bar graph. For immunofluorescence, sections were additionally stained with DAPI for the nucleus.

Confocal fluorescent images were taken with Leica TCS SPE (Leica Microsystems Inc.) at Stanford Cell Sciences Imaging Facility (NIH SIG 1S10OD010558001A1) Oil red O staining was performed on cryosections from fresh liver tissues embedded and frozen in Optimal Cutting Temperature Compound. The slides were fixed in 10% neutral buffered formalin (Research Products International) for 30 min. After washing with water, the slides were placed in 100% propylene glycol (Poly Scientific) for 5 min and 85% propylene glycol for another 5 min. The slides were stained for oil red o stain (Frontier Scientific) preheated at 60°C for 10 min, and differentiated in 85% propylene glycol for 3 min. The slides were counterstained with hematoxylin stain, Harris for 30 sec and bluing solution for 10 dips.

SA-β-galactosidase staining assay. Fresh liver tissues were embedded and frozen in Optimal Cutting Temperature Compound, and sectioned for staining. The staining was performed following the manufacturer's protocol (Millipore).

Lucigenin assay. ROS production was studied using lucigenin assay. Fresh liver tissues or transfected primary hepatocytes were homogenized on ice in sucrose buffer (0.3 M sucrose, 10 mM HEPES, 10 mM KCl, 0.1 mM EDTA, 0.1 mM EGTA, 0.5 mM Spermidine, 1 mM DTT, pH 7.4) with protease inhibitors (Roche, Basel, Switzerland), and centrifuged at 1000 g for 5 minutes. The supernatant was further centrifuged at 100,000g for 1 hour at 4°C to obtain membrane-enriched fractions. The pellet was suspended in Krebs buffer (100 mM NaCl, 5 mM KCl, 2 mM $CaCl_2$, 1.2 mM $MgSO_4$, 1.0 mM K_2HPO_4, 25 mM $NaHCO_3$, 20 mM Na-HEPES, 0.2% glucose, pH 7.4) with PI. Membrane fractions were incubated with lucigenin (5 uM, Invitrogen) at room temperature for 15 min. then 100 uM of NADPH (Sigma-Aldrich) was added and the chemiluminescence intensity was read with Pharmingen Monolight 3010

luminometer (BD, Franklin Lakes, NJ) every 1 minute, up to 10 counts. Data were normalized to the protein concentration.

Triglyceride (TG) content. Liver triglycerides were measured by using the triglyceride colorimetric assay kit (Cayman Chemical, Ann Arbor, MI) following the manufacturer's instructions. Liver tissue was homogenized in diluent buffer containing protease inhibitors before centrifugation at 1,000 g for 10 minutes at 4°C. The samples and the standards were added to a 96 well plate to react with the enzyme solution for 15 minutes and the absorbance was measured at 530-550 nm.

Real-time polymerase chain reaction (PCR). RNA from cells or tissues was extracted with RNeasy Mini kit (QIAGEN, Germantown, MD). One ug of RNA was reverse-transcribed (iScriptTM cDNA synthesis kit, Bio-Rad, Hercules, CA) and RT-qPCR was performed on the 7900 HT system (Applied Biosystems- Thermo Fisher Scientific, Waltham, MA) using Power SYBR Green PCR Master Mix (Applied Biosystems). Following normalization to housekeeping genes, relative quantification was performed to analyze the data. The primer sequences are listed in Supplementary Table 2.

Western blotting and immunoprecipitation. Liver tissue samples were homogenized in radioimmunoprecipitation assay (RIPA) buffer supplemented with cOmplete™ protease inhibitor cocktail (Roche). Following centrifugation at 10,000 g for 10 minutes at 4°C, samples were subjected to 10% SDS-polyacrylamide gel electrophoresis (SDS-PAGE) and transferred onto nitrocellulose membranes, after blocking membranes were incubated with primary antibodies overnight at 4°C, then with appropriate horseradish peroxidase-conjugated secondary antibodies. Detection was performed by chemiluminescence method. Protein expression quantification was done using NIH ImageJ.

Primary hepatocytes were serum-starved overnight prior to treatment with 200 uM palmitate or control BSA for 1 hour. Cells were washed in cold PBS and lysates were collected in RIPA buffer supplemented with protease and phosphatase inhibitor cocktails (Roche) on ice. Immunoprecipitation of tissue homogenates or cell lysates was performed using Pierce™ Protein A/G Magnetic Beads (Thermo Fisher Scientific) according to manufacturer protocol. Equal amounts of protein lysate were incubated with bead-antibody complex. Following elution, samples were analyzed by western blotting. Primary and secondary antibodies used are listed in Supplementary Table 3.

Proximity ligation assay. Duolink Proximity Ligation assay kit (Sigma-Aldrich) was used to determine the interaction of Nox2 subunit $p47^{phox}$ and p52Shc in hepatocytes isolated from young and old mice. Reagents were used following manufacturer's instruction and steps were optimized. In brief, rabbit polyclonal anti-Shc (Abcam) and mouse monoclonal anti-$p47^{phox}$ (Santa Cruz Biotechnology, Dallas, TX) were used. A pair of oligonucleotide-labeled secondary antibodies (PLA probes) were bound to the primary antibodies, and the hybridizing connector oligoes joined the PLA probes if they were in close proximity and the ligase forming a DNA template that was required for rolling-circle amplification (RCA). Labeled oligos hybridized to the complementary sequences within the amplicon, which were then visualized and quantified as discrete red fluorescent signals by confocal microscopy (Leica Microsystems Inc.). NIH Image J software was used to count the signal and the average counts were used to plot the bar graph.

Generation of the p52ShcδPTB and p52ShcδSH2 constructs and cell transfection. Deletion mutants of human wild type p52Shc were prepared based on the construct harboring the p52Shc ORF N-terminally fused to the Avi-tag and harboring the biotin ligase under control of CVM promoter (GeneCopoeia, INC., Rockville, MD). To create the deletion mutant p52Shc-Δ(44-

198)PTB we used following primers 5'-GTCGTTGGGATGCAGCCAGCC-3'and 5'-GAGTTGCGCTTCAAACAATACCTC-3'. For deletion of the (329-425) SH2 domain we used 5'-GAGCTGCTCAGCCATGGACAC-3' and 5'-GAGCGGAAACTGTACCTCGAGT-3'. All mutants were verified by sequencing analysis and by the Western Blots with domain-specific antibody. Primary hepatocytes were transfected with wild type or p52ShcδSH2 constructs by JetPEI (Polyplus Transfection, New York, NY) per manufacturer protocol for 24 hours. Following overnight serum starvation, the cells were treated with 200 uM palmitate or control BSA for 16 hours. Treated cells were collected in sucrose buffer and ROS production was measured as described above.

Binding models of $p47^{phox}$ and p52Shc. RosettaCM as described (17) was utilized to construct the $p47^{phox}$ and p52Shc full-atomic models. Three pieces of X-ray structural templates: 1KQ6 which covers the PX domain, 1OV3 which covers the SH3 domain, and 1K4U which covers the C-terminus were used to assemble the $p47^{phox}$ structure, the regions that were structurally missing were then filled with ROBETTA server of 3-mers and 9-mers structural sequence library. Backbone optimization and fragment insertions were carried out via centroid energy function. Third, low-energy side chain construction and placement were done iteratively using FASTRELAX protocol with the latest ROSETTA energy scoring function, talaris2014. Similarly, p52Shc was built using the same protocol with two pieces of X-ray structural templates: 1OY2 which covers the PTB domain, and 1MIL which covers the SH2 domain with the ROBETTA server of 3-mers and 9-mers fragments for the regions not covered by the templates. RosettaDock 3 protocol was utilized for docking the two homology models. The SH2 of p52Shc which is believed to interact with $p47^{phox}$ was placed nearby the $p47^{phox}$ protein. Second, p52Shc and $p47^{phox}$ are translated 3 Å, and rotated 8° around each other per cycle to

locate the interface. Then the docked poses with the lowest energy state is constructed with full-atomic side chains and refined. 150 rounds of decoys are generated and minimized and each one is visualized using PYMOL.

References:

1. Bettaieb A, Jiang JX, Sasaki Y, Chao TI, Kiss Z, Chen X, et al. Hepatocyte Nicotinamide Adenine Dinucleotide Phosphate Reduced Oxidase 4 Regulates Stress Signaling, Fibrosis, and Insulin Sensitivity During Development of Steatohepatitis in Mice. Gastroenterology. 2015;149(2):468-80 e10.
2. Geerts A, Niki T, Hellemans K, De Craemer D, Van Den Berg K, Lazou JM, et al. Purification of rat hepatic stellate cells by side scatter-activated cell sorting. Hepatology. 1998;27(2):590-8.
3. Zigmond E, Samia-Grinberg S, Pasmanik-Chor M, Brazowski E, Shibolet O, Halpern Z, et al. Infiltrating monocyte-derived macrophages and resident kupffer cells display different ontogeny and functions in acute liver injury. J Immunol. 2014;193(1):344-53.